Results in Physics 72 (2025) 108203

Contents lists available at ScienceDirect

Results in Physics

journal homepage: www.elsevier.com/locate/rinp

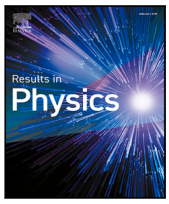

Chaotic analysis and a damped oscillator solitary wave structures to the generalized reaction Duffing model

Ghulam Hussain Tipu [a,b,*], Waqas Ali Faridi [c], Muhammad Bilal Riaz [d,e], Fengping Yao [a,b], Usman Younas [a,b], Mubariz Garayev [f]

[a] Department of Mathematics, Shanghai University, No. 99 Shangda Road, Shanghai 200444, China
[b] Newtouch Center for Mathematics of Shanghai University, Shanghai 200444, China
[c] Department of Mathematics, University of Management and Technology, Lahore, Pakistan
[d] IT4Innovations, VSB - Technical University of Ostrava, Ostrava, Czech Republic
[e] Jadara University Research Center, Jadara University, Jordan
[f] Department of Mathematics, College of Science, King Saud University, P.O. Box 2455, Riyadh, Saudi Arabia

ARTICLE INFO

Keywords:
The generalized reaction Duffing model
The Kumar–Malik method
Analytical solutions
Jacobi elliptic functions
Chaotic analysis

ABSTRACT

The aim of this research is to obtain soliton solutions for the generalized reaction Duffing model, a framework that generalizes many important models that illustrate key phenomena in science and engineering. In contrast to regular harmonic motion, this equation describes the motion of a damped oscillator with a more complex potential. We used the Kumar–Malik method in this work to obtain analytical solutions for the generalized reaction Duffing model, which is the first time this method has been used to extract soliton solutions in this particular setting. The equation is first reformulated as a nonlinear ordinary differential equation using traveling wave transformation. The approach proves particularly effective in handling nonlinear partial differential equations, yielding hyperbolic, Jacobi elliptic, trigonometric, and exponential function solutions under appropriate parameter constraints. A variety of innovative solutions emerge, including periodic wave solutions, dark compacton waves, kink waves, singular kink waves, bright solitons, breather waves, and singular-shaped solitons via the Kumar–Malik method. The solutions are then shown visually to demonstrate the wave behavior under various conditions. Our findings enhance the comprehension of the Duffing equation's behavior across different physical contexts. The research uses extensive 2D and 3D graphic plot solutions of the proposed solutions for a better graphical understanding of the physical perimeters of solutions and proves the feasibility of the proposed method in solving complex nonlinear equations. The Chaotic analysis has also been discussed by perturbation term and initial conditions. It is important to note that the proposed methods are competent, credible, and interesting analytical tools for solving nonlinear partial differential equations. In addition, these solutions represent a valuable resource for the understanding of the complex behavior of physical systems, as well as for inspiring future research.

Introduction

Nonlinear evolution equations (NLEEs) represent many real-world phenomena [1,2]. The analysis of these equations is made difficult due to their inherent nonlinear characteristics, such that even very small changes in governing parameters can result in significant changes in their behavior. This complexity calls for definitive solutions of NLEEs. Traveling wave (TW) solutions to nonlinear partial differential equations (NLPDEs) have proved to be precise solutions that are crucial to advancing many scientific and engineering disciplines [3]. Investigation of nonlinear physical processes, including low pressure wave propagation, chemical dynamics, geochemistry, computational physics, plasma physics, fluid mechanics, quantum field theory, etc., require these solutions [4–10].

Numerous nonlinear evolution equations define analytical solutions to these intricate processes, which spark intense interest in the mathematical community to create robust and effective techniques for locating analytical solutions [11]. The particular NLEE types that only offer responses based on particular combinations of elements (such as TW variables) are particularly noteworthy. In order to simulate the propagation of strong laser pulses across nonlinear optical medium and study phenomena like self-phase modulation and soliton self-focusing,

* Corresponding author.
E-mail address: gh.tipu67@gmail.com (G.H. Tipu).

https://doi.org/10.1016/j.rinp.2025.108203
Received 2 December 2024; Received in revised form 13 February 2025; Accepted 11 March 2025
Available online 19 March 2025

complex soliton solutions are necessary. Fiber optics for long-distance communication applications need soliton technology [12,13].

Nonlinear partial differential equations are crucial for modeling many mathematical physical systems, involving the derivation of analytical solutions. Durable methodologies produced effective techniques for treating NLPDEs. The primary approaches used include the ϕ^6 model expansion method [14–16], the Hirota bilinear method [17,18], the innovative Kudryashov approach [19,20], and a novel auxiliary equation method [21]. Ultimately, the expansion technique for the sinh-Gordon equation [22], the Modified Exp-function and Kudryashov methods [23,24], the generalized Riccati equation mapping (GREMM) method [25–27], the q-HATM techniques [28], the Khater II method [29], and the Sardar Sub equation method [29] constitute additional significant methodologies. The notable contributions include the generalized Khater (GK) technique employing Atangana's conformable fractional derivative operator [30], the auto-Backlund transformation method [31], Jacobi elliptic function techniques [32], the Jacobi elliptic function expansion (JEFE) method [33], the modified exponential rational functional method [34], and the undetermined coefficients method [35]. These methods increase the accuracy in solving such complex equations while at the same time increasing the computational efficiencies.

The generalized reaction Duffing model (GRDM) is a significant mathematical framework available in physics. The Duffing equation is a description of a problem of cubic nonlinearity that was first published in a comprehensive treatise by the German engineer George Duffing in 1918 [36]. It is seen that this equation possesses a broad range of established properties in nonlinear dynamical systems and provides an important tool for researchers studying such systems. It has been the object of attention from chaos theorists since the 1970s as one of the simplest equations presenting chaotic behavior in dynamical systems. In [37], the chaotic dynamics of the fractionally damped Duffing equation are discussed. Furthermore, in shallow regions above a flat seafloor, nonlinear models such as the GRDM exhibit notable spectral energy transfer for finite amplitude waves. In mechanical contexts, the Duffing equation is adept at modeling nonlinear vibrations, particularly in mechanical structures subjected to external forces or excitations.

Recently in (2024), Cortez et al. [38] studied the generalized reaction Duffing equation and developed traveling wave solutions by using mapping method and Bernoulli sub-ODE approach. Tariq et al. [39] derived the fractional solitons by using extended modified auxiliary equation mapping method for the considered model. Razzaq et al. [40] utilized modified $\frac{G'}{G^2}$−expansion method and construed some analytical exact solution of the generalized reaction Duffing equation. In (2025), said et al. [41] applied the Sardar Sub-equation method and established soliton solutions for the considered model. This on going study inspired me to conduct this study because all utilized techniques in above-mentioned study constructed soliton solutions with trigonometric and hyperbolic functions, but the solutions with Jacobi elliptic function for the considered model were missing and gap in literature. Secondly, there is not existing study on generalized reaction-Duffing equation in which chaos analysis studied. Thus, in order to fill this study gap, this study is carried out and generalized reaction-Duffing equation is investigating by the Kumar–Malik method that is developed recently in (2024), based on the first-order differential equation introduced by Kumar and Malik [42] which enable us to develop Jacobi elliptic function based solutions. The solutions manifest as Jacobian elliptic function, hyperbolic, trigonometric, and exponential functions, illustrating the extensive applicability of these techniques. Notably, these results have not been established in previous studies because the Kumar–Malik method has not been used to find exact solutions for GRDM until now. On the other hand, the dynamical aspects are also displaying by using the chaos analysis. However, variational method, Kudryashov method, Sardar sub-equation, and the bilinear method are also powerful approaches which can use to find soliton solutions such as, Wang [43,44] utilized variational and the bilinear methods to develop soliton solutions for B-type Kadomtsev–Petviashvili and Chou et al. [45,46] used Kudryashov's method and Sardar sub-equation method to construct soliton solutions.

The paper is organized as follows: Section "Description of Kumar–Malik method" outlines the Kumar–Malik method core algorithm, respectively. In Section "Application of the method", the paper derives exact solutions for the generalized reaction Duffing model using the proposed technique. The graphical demonstration is presented in Section "Graphical representation and its behavior". We discuss the chaotic analysis in Section "Chaotic analysis". The paper concludes in Section "Conclusion".

Description of Kumar–Malik method

In this section, we outline the Kumar–Malik method to solve the Duffing model of the generalized reaction.

Suppose the following non-linear evolution equation for $S(x,t)$:

$$\Pi(S, S_x, S_t, S_{xx}, S_{tt}, \ldots) = 0, \tag{1}$$

Step 1. Using the wave transformation technique:

$$S(x,t) = \Psi(\psi), \ \psi = n_0 x - kt, \tag{2}$$

where n_0 and k denote wave number and velocity, respectively. Substituting Eq. (2) in Eq. (1) yields an ODE for $\Psi(\psi)$:

$$\Delta(\Psi, \Psi', \Psi'', \Psi''', \Psi'''', \ldots) = 0, \tag{3}$$

the exponents of Ψ indicate differentiation with respect to ψ.

Step 2. Consider the solution for Eq. (3) to take the following form:

$$\Psi(\psi) = \mu_0 + \mu_1 Y(\psi) + \mu_2 Y(\psi)^2 + \cdots \ldots + \mu_M Y(\psi)^N, \tag{4}$$

where the constants μ_i $(i = 1, 2, \ldots, M)$ are undetermined, and the function $Y(\psi)$ is subject to the first-order ODE:

$$Y'(\psi) = \sqrt{\xi_1 Y(\psi)^4 + \xi_2 Y(\psi)^3 + \xi_3 Y(\psi)^2 + \xi_4 Y(\psi) + \xi_5}, \tag{5}$$

where $\xi_j' s (j = 1, 2, 3, 4, 5)$ are arbitrary constants.

Step 3. To determine N in Eq. (3), we apply balancing techniques, equating the highest-order derivative with the highest-degree nonlinear term to attain equilibrium within the equation.

Step 4. Substituting Eq. (4) and its derivatives from Eq. (5) into Eq. (3) yields a polynomial in $Y(\psi)Y'(\psi)$. By organizing the coefficients of each power and setting them to zero, we derive a system of equations to get the values of unknown parameters K_0, $\mu_i (i = 1, 2, \ldots, N)$, and $\xi_j (j = 1, 2, 3, 4, 5)$. The solutions to this system provide the exact solutions to Eq. (3).

Step 5. The solutions of Eq. (3) and the transformation in Eq. (2) yield multiple exact solutions for the NLPDE in Eq. (1).

Solutions of Eq. (5)

Case 1: When $\xi_4 = \frac{\xi_2(4\xi_1\xi_3 - \xi_2^2)}{8\xi_1^2}$ and $\xi_5 = 0$, the general solution to Eq. (5) is expressed in terms of Jacobi elliptic functions:

Sub-case 1.1: If $\xi_1 < 0, \ (4\xi_1\xi_3 - \xi_2^2) > 0$.

$$Y_1(\psi) = -\frac{\xi_2}{4\xi_1} \pm \frac{\xi_2}{4\xi_1} cn\left(\frac{\sqrt{-\xi_1(4\xi_1\xi_3 - \xi_2^2)}}{2\xi_1}\psi, \frac{\xi_2}{2\sqrt{(4\xi_1\xi_3 - \xi_2^2)}}\right), \tag{6}$$

$$Y_2(\psi) = -\frac{\xi_2}{4\xi_1} \pm \frac{\xi_2}{4\xi_1} dn\left(\frac{\xi_2}{4\sqrt{-\xi_1}}\psi, \frac{2\sqrt{(4\xi_1\xi_3 - \xi_2^2)}}{\xi_2}\right). \tag{7}$$

Sub-case 1.2: If $\xi_1 < 0, \ (4\xi_1\xi_3 - \xi_2^2) < 0, \ (16\xi_1\xi_3 - 5\xi_2^2) < 0$.

$$Y_3(\psi) = -\frac{\xi_2}{4\xi_1} \pm \frac{\sqrt{-(16\xi_1\xi_3 - 5\xi_2^2)}}{4\xi_1} cn$$

$$\times\left(\frac{\sqrt{\xi_1(4\xi_1\xi_3-\xi_2^2)}}{2\xi_1}\psi,\frac{\sqrt{(4\xi_1\xi_3-\xi_2^2)(16\xi_1\xi_3-5\xi_2^2)}}{2(4\xi_1\xi_3-\xi_2^2)}\right), \tag{8}$$

$$Y_4(\psi)=-\frac{\xi_2}{4\xi_1}\pm\frac{\sqrt{-(16\xi_1\xi_3-5\xi_2^2)}}{4\xi_1}\,dn \times\left(\frac{\sqrt{\xi_1(16\xi_1\xi_3-5\xi_2^2)}}{4\xi_1}\psi,\frac{2\sqrt{(4\xi_1\xi_3-\xi_2^2)(16\xi_1\xi_3-5\xi_2^2)}}{(16\xi_1\xi_3-5\xi_2^2)}\right). \tag{9}$$

Sub-case 1.3: If $\xi_1<0,\ (4\xi_1\xi_3-\xi_2^2)>0,\ (16\xi_1\xi_3-5\xi_2^2)<0$.

$$Y_5(\psi)=-\frac{\xi_2}{4\xi_1}\pm\frac{\sqrt{-(16\xi_1\xi_3-5\xi_2^2)}}{4\xi_1}\,nc \times\left(\frac{\sqrt{-\xi_1(4\xi_1\xi_3-\xi_2^2)}}{2\xi_1}\psi,\frac{\xi_2}{2\sqrt{(4\xi_1\xi_3-\xi_2^2)}}\right), \tag{10}$$

$$Y_6(\psi)=-\frac{\xi_2}{4\xi_1}\pm\frac{\sqrt{-(16\xi_1\xi_3-5\xi_2^2)}}{4\xi_1}\,nd\left(\frac{\xi_2}{4\sqrt{-\xi_1}}\psi,\frac{2\sqrt{(4\xi_1\xi_3-\xi_2^2)}}{\xi_2}\right). \tag{11}$$

Sub-case 1.4: If $(4\xi_1\xi_3-\xi_2^2)>0,\ (4\xi_1\xi_3-\xi_2^2)(16\xi_1\xi_3-5\xi_2^2)>0$.

$$Y_7(\psi)=-\frac{\xi_2}{4\xi_1}\pm\frac{\xi_2}{4\xi_1}\,nc \times\left(\frac{\sqrt{\xi_1(4\xi_1\xi_3-\xi_2^2)}}{2\xi_1}\psi,\frac{\sqrt{(4\xi_1\xi_3-\xi_2^2)(16\xi_1\xi_3-5\xi_2^2)}}{2(4\xi_1\xi_3-\xi_2^2)}\right), \tag{12}$$

$$Y_8(\psi)=-\frac{\xi_2}{4\xi_1}\pm\frac{\xi_2}{4\xi_1}\,nd \times\left(\frac{\sqrt{\xi_1(16\xi_1\xi_3-5\xi_2^2)}}{4\xi_1}\psi,\frac{2\sqrt{(4\xi_1\xi_3-\xi_2^2)(16\xi_1\xi_3-5\xi_2^2)}}{(16\xi_1\xi_3-5\xi_2^2)}\right). \tag{13}$$

Sub-case 1.5: If $\xi_1>0,\ (16\xi_1\xi_3-5\xi_2^2)<0$.

$$Y_9(\psi)=-\frac{\xi_2}{4\xi_1}\pm\frac{\xi_2}{4\xi_1}\,ns\left(\frac{\xi_2}{4\sqrt{\xi_1}}\psi,\frac{\sqrt{-(16\xi_1\xi_3-5\xi_2^2)}}{\xi_2}\right), \tag{14}$$

$$Y_{10}(\psi)=-\frac{\xi_2}{4\xi_1}\pm\frac{\sqrt{-(16\xi_1\xi_3-5\xi_2^2)}}{4\xi_1}\,ns \times\left(\frac{\sqrt{-\xi_1(16\xi_1\xi_3-5\xi_2^2)}}{4\xi_1}\psi,\frac{\xi_2}{\sqrt{-(16\xi_1\xi_3-5\xi_2^2)}}\right), \tag{15}$$

$$Y_{11}(\psi)=-\frac{\xi_2}{4\xi_1}\pm\frac{\sqrt{-(16\xi_1\xi_3-5\xi_2^2)}}{4\xi_1}\,sn\left(\frac{\xi_2}{4\sqrt{\xi_1}}\psi,\frac{\sqrt{-(16\xi_1\xi_3-5\xi_2^2)}}{\xi_2}\right), \tag{16}$$

$$Y_{12}(\psi)=-\frac{\xi_2}{4\xi_1}\pm\frac{\xi_2}{4\xi_1}\,sn\left(\frac{\sqrt{-\xi_1(16\xi_1\xi_3-5\xi_2^2)}}{4\xi_1}\psi,\frac{\xi_2}{\sqrt{-(16\xi_1\xi_3-5\xi_2^2)}}\right). \tag{17}$$

In Jacobi elliptic functions, the second argument is the modulus, e.g., $sn(\psi,q)$.

Case 2: When $\xi_4=\frac{\xi_2(4\xi_1\xi_3-\xi_2^2)}{8\xi_1^2}$ and $\xi_5=\frac{(4\xi_1\xi_3-\xi_2^2)^2}{64\xi_1^3}$, Eq. (5) exhibits hyperbolic and trigonometric solutions, where $\mathfrak{X}=8\xi_1\xi_3-3\xi_2^2$.

Sub-case 2.1: If $\xi_1>0,\ \mathfrak{X}<0$.

$$Y_{13}(\psi)=-\frac{\xi_2}{4\xi_1}\pm\frac{\sqrt{-\mathfrak{X}}}{4\xi_1}\tanh\left(\frac{\sqrt{-\xi_1\mathfrak{X}}}{4\xi_1}\psi\right), \tag{18}$$

$$Y_{14}(\psi)=-\frac{\xi_2}{4\xi_1}\pm\frac{\sqrt{-\mathfrak{X}}}{4\xi_1}\coth\left(\frac{\sqrt{-\xi_1\mathfrak{X}}}{4\xi_1}\psi\right), \tag{19}$$

Sub-case 2.2: If $\xi_1>0,\ \mathfrak{X}>0$.

$$Y_{15}(\psi)=-\frac{\xi_2}{4\xi_1}\pm\frac{\sqrt{\mathfrak{X}}}{4\xi_1}\tan\left(\frac{\sqrt{\xi_1\mathfrak{X}}}{4\xi_1}\psi\right), \tag{20}$$

$$Y_{16}(\psi)=-\frac{\xi_2}{4\xi_1}\pm\frac{\sqrt{\mathfrak{X}}}{4\xi_1}\cot\left(\frac{\sqrt{\xi_1\mathfrak{X}}}{4\xi_1}\psi\right), \tag{21}$$

Case 3: When $\xi_4=\frac{\xi_2(4\xi_1\xi_3-\xi_2^2)}{8\xi_1^2}$ and $\xi_5=\frac{\xi_2^2(16\xi_1\xi_3-5\xi_2^2)}{256\xi_1^3}$, Eq. (5) exhibits hyperbolic and trigonometric solutions:

Sub-case 3.1: If $\xi_1<0,\ \mathfrak{X}<0$.

$$Y_{17}(\psi)=-\frac{\xi_2}{4\xi_1}\pm\frac{\sqrt{-2\mathfrak{X}}}{4\xi_1}\,sech\left(\frac{\sqrt{2\xi_1\mathfrak{X}}}{4\xi_1}\psi\right). \tag{22}$$

Sub-case 3.2: If $\xi_1>0,\ \mathfrak{X}>0$.

$$Y_{18}(\psi)=-\frac{\xi_2}{4\xi_1}\pm\frac{\sqrt{2\mathfrak{X}}}{4\xi_1}\,csch\left(\frac{\sqrt{2\xi_1\mathfrak{X}}}{4\xi_1}\psi\right). \tag{23}$$

Sub-case 3.3: If $\xi_1>0,\ \mathfrak{X}<0$.

$$Y_{19}(\psi)=-\frac{\xi_2}{4\xi_1}\pm\frac{\sqrt{-2\mathfrak{X}}}{4\xi_1}\sec\left(\frac{\sqrt{-2\xi_1\mathfrak{X}}}{4\xi_1}\psi\right). \tag{24}$$

$$Y_{20}(\psi)=-\frac{\xi_2}{4\xi_1}\pm\frac{\sqrt{-2\mathfrak{X}}}{4\xi_1}\csc\left(\frac{\sqrt{-2\xi_1\mathfrak{X}}}{4\xi_1}\psi\right). \tag{25}$$

Case 4: Substituting $\xi_2=\xi_4=\xi_5=0$ and $\xi_3>0$ yields a solution to Eq. (5) in the following form:

$$Y_{21}(\psi)=\frac{4\rho\xi_3}{\left(4\rho^2e^{\sqrt{\xi_3}\psi}-\xi_1\xi_3e^{-\sqrt{\xi_3}\psi}\right)}, \tag{26}$$

by taking $\xi_1=-\frac{4\rho^2}{\xi_3}$, solution Eq. (26) reduces to

$$Y_{22}(\psi)=\frac{\xi_3}{2\rho}sech(-\sqrt{\xi_3}\psi), \tag{27}$$

while by taking $\xi_1=\frac{4\rho^2}{\xi_3}$, solution Eq. (27) reduces to

$$Y_{23}(\psi)=\frac{\xi_3}{2\rho}csch(-\sqrt{\xi_3}\psi). \tag{28}$$

The generalized reaction-Duffing model

The generalized reaction Duffing model as follows [38]:

$$S_{tt}+\delta S_{xx}+\omega S+pS^2+\kappa S^3=0,\quad t>0, \tag{29}$$

where δ, ω, p, and κ are constants. If $p=0$, then Eq. (1) converts into,

$$S_{tt}+\delta S_{xx}+\omega S+\kappa S^3=0. \tag{30}$$

The model depicts the motion of a damped oscillator with a more complex potential than in basic harmonic motion. The addition of quadratic and cubic nonlinear elements enables the model to describe a wide range of oscillatory behaviors, including hardening and softening spring effects. The term δS_{xx} represents spatial diffusion or dispersion, allowing the model to simulate wave propagation in different mediums. The simplified equation continues to model a nonlinear wave but does not include the quadratic interaction element. This could indicate instances in which the wave's amplitude has no substantial effect on its quadratic propagation. However, the cubic term enables for the investigation of wave behaviors such as solitary waves or other types of

nonlinearity, but with potentially different dynamics than the original equation. Let us consider the traveling wave transformation as:

$$S(x,t) = \Psi(\psi),\ \psi = n_0\, x - kt, \tag{31}$$

where n_0 and k denote wave number and velocity, respectively. Substituting Eq. (31) in Eq. (30) yields an ODE for $\Psi(\psi)$:

$$(k^2 + \delta n_0^2)\Psi'' + \omega\Psi + \kappa\Psi^3 = 0. \tag{32}$$

Application of the method

In order to find the soliton solutions, Balancing the highest-order derivative Ψ'' with the nonlinear term Ψ^3 from Eq. (32) results in $N = 1$. Therefore, for $N = 1$, Eq. (4) simplifies to

$$\Psi(\psi) = \mu_0 + \mu_1 Y(\psi), \tag{33}$$

by substituting Eq's. (5) and (33) into Eq. (32) and equating each coefficient of $Y(\psi)(i = 0, 1, 2, 3)$ to zero, the resulting expressions are derived as follows:

$$\begin{aligned}
&(Y(\psi))^0 : \frac{1}{2}\mu_1\xi_4\delta n_0^2 + \frac{1}{2}\mu_1\xi_4 k^2 + \omega\mu_0 + \kappa\mu_0^3 = 0,\\
&(Y(\psi))^1 : \delta\mu_1 n_0^2\xi_3 + k^2\mu_1\xi_3 + 3\kappa\mu_0^2\mu_1 + \omega\mu_1 = 0,\\
&(Y(\psi))^2 : \frac{3}{2}\mu_1\xi_2\delta n_0^2 + \frac{3}{2}\mu_1\xi_2 k^2 + 3\kappa\mu_0\mu_1^2 = 0,\\
&(Y(\psi))^3 : 2\delta\mu_1 n_0^2\xi_1 + 2k^2\mu_1\xi_1 + \kappa\mu_1^3 = 0.
\end{aligned} \tag{34}$$

The Maple program is used and applied on the given system to find the solution and get results.

Case 1: Under the parameters $\xi_4 = \frac{\xi_2(4\xi_1\xi_3-\xi_2^2)}{8\xi_1^2}$, $\xi_5 = 0$ the solution of system (34) is,

$$\mu_0 = \pm\sqrt{\frac{\omega}{\kappa\,\mathfrak{X}}}\,\xi_2, \quad \mu_1 = \pm 4\sqrt{\frac{\omega}{\kappa\,\mathfrak{X}}}\,\xi_1, \quad \delta = -\frac{k^2\mathfrak{X} + 8\omega\xi_1}{n_0^2\,\mathfrak{X}}, \tag{35}$$

where $\mathfrak{X} = 8\xi_1\xi_3 - 3\xi_2^2$.

Substituting into (33) and applying (6)–(17), the elliptic Jacobi solutions of (30) are obtained:

$$S(x,t) = \Psi(\psi) = \pm\sqrt{\frac{\omega}{\kappa\,\mathfrak{X}}}\,\xi_2 \pm 4\sqrt{\frac{\omega}{\kappa\,\mathfrak{X}}}\,\xi_1 Y(\psi). \tag{36}$$

Sub-case 1.1: If $\xi_1 < 0,\ (4\xi_1\xi_3 - \xi_2^2) > 0.$

$$S_1(x,t) = \pm\sqrt{\frac{\omega}{\kappa\,\mathfrak{X}}}\,\xi_2\, cn\left(\frac{\sqrt{-\xi_1(4\xi_1\xi_3-\xi_2^2)}}{2\xi_1}\psi, \frac{\xi_2}{2\sqrt{(4\xi_1\xi_3-\xi_2^2)}}\right), \tag{37}$$

the periodic wave solution of (37) is illustrated in Fig. 1.

$$S_2(x,t) = \pm\sqrt{\frac{\omega}{\kappa\,\mathfrak{X}}}\,\xi_2\, dn\left(\frac{\xi_2}{4\sqrt{-\xi_1}}\psi, \frac{2\sqrt{(4\xi_1\xi_3-\xi_2^2)}}{\xi_2}\right). \tag{38}$$

Sub-case 1.2: If $\xi_1 < 0,\ (4\xi_1\xi_3 - \xi_2^2) < 0,\ (16\xi_1\xi_3 - 5\xi_2^2) < 0.$

$$\begin{aligned}
S_3(x,t) &= \pm\sqrt{\frac{-\omega\,(16\xi_1\xi_3-5\xi_2^2)}{\kappa\,\mathfrak{X}}}\, cn\\
&\times\left(\frac{\sqrt{\xi_1(4\xi_1\xi_3-\xi_2^2)}}{2\xi_1}\psi, \frac{\sqrt{(4\xi_1\xi_3-\xi_2^2)(16\xi_1\xi_3-5\xi_2^2)}}{2(4\xi_1\xi_3-\xi_2^2)}\right),
\end{aligned} \tag{39}$$

$$\begin{aligned}
S_4(x,t) &= \pm\sqrt{\frac{-\omega\,(16\xi_1\xi_3-5\xi_2^2)}{\kappa\,\mathfrak{X}}}\, dn\\
&\times\left(\frac{\sqrt{\xi_1(16\xi_1\xi_3-5\xi_2^2)}}{4\xi_1}\psi, \frac{2\sqrt{(4\xi_1\xi_3-\xi_2^2)(16\xi_1\xi_3-5\xi_2^2)}}{(16\xi_1\xi_3-5\xi_2^2)}\right).
\end{aligned} \tag{40}$$

Sub-case 1.3: If $\xi_1 < 0,\ (4\xi_1\xi_3 - \xi_2^2) > 0,\ (16\xi_1\xi_3 - 5\xi_2^2) < 0.$

$$\begin{aligned}
S_5(x,t) &= \pm\sqrt{\frac{-\omega\,(16\xi_1\xi_3-5\xi_2^2)}{\kappa\,\mathfrak{X}}}\, nc\\
&\times\left(\frac{\sqrt{-\xi_1(4\xi_1\xi_3-\xi_2^2)}}{2\xi_1}\psi, \frac{\xi_2}{2\sqrt{(4\xi_1\xi_3-\xi_2^2)}}\right),
\end{aligned} \tag{41}$$

$$S_6(x,t) = \pm\sqrt{\frac{-\omega\,(16\xi_1\xi_3-5\xi_2^2)}{\kappa\,\mathfrak{X}}}\, nd\left(\frac{\xi_2}{4\sqrt{-\xi_1}}\psi, \frac{2\sqrt{(4\xi_1\xi_3-\xi_2^2)}}{\xi_2}\right). \tag{42}$$

Sub-case 1.4: If $(4\xi_1\xi_3 - \xi_2^2) > 0,\ (4\xi_1\xi_3 - \xi_2^2)(16\xi_1\xi_3 - 5\xi_2^2) > 0.$

$$\begin{aligned}
S_7(x,t) &= \pm\sqrt{\frac{\omega}{\kappa\,\mathfrak{X}}}\,\xi_2\, nc\\
&\times\left(\frac{\sqrt{\xi_1(4\xi_1\xi_3-\xi_2^2)}}{2\xi_1}\psi, \frac{\sqrt{(4\xi_1\xi_3-\xi_2^2)(16\xi_1\xi_3-5\xi_2^2)}}{2(4\xi_1\xi_3-\xi_2^2)}\right),
\end{aligned} \tag{43}$$

$$\begin{aligned}
S_8(x,t) &= \pm\sqrt{\frac{\omega}{\kappa\,\mathfrak{X}}}\,\xi_2\, nd\\
&\times\left(\frac{\sqrt{\xi_1(16\xi_1\xi_3-5\xi_2^2)}}{4\xi_1}\psi, \frac{2\sqrt{(4\xi_1\xi_3-\xi_2^2)(16\xi_1\xi_3-5\xi_2^2)}}{(16\xi_1\xi_3-5\xi_2^2)}\right).
\end{aligned} \tag{44}$$

Sub-case 1.5: If $\xi_1 > 0,\ (16\xi_1\xi_3 - 5\xi_2^2) < 0.$

$$S_9(x,t) = \pm\sqrt{\frac{\omega}{\kappa\,\mathfrak{X}}}\,\xi_2\, ns\left(\frac{\xi_2}{4\sqrt{\xi_1}}\psi, \frac{\sqrt{-(16\xi_1\xi_3-5\xi_2^2)}}{\xi_2}\right), \tag{45}$$

the dark compacton wave solution of (45) is illustrated in Fig. 2.

$$\begin{aligned}
S_{10}(x,t) &= \pm\sqrt{\frac{-\omega\,(16\xi_1\xi_3-5\xi_2^2)}{\kappa\,\mathfrak{X}}}\, ns\\
&\times\left(\frac{\sqrt{-\xi_1(16\xi_1\xi_3-5\xi_2^2)}}{4\xi_1}\psi, \frac{\xi_2}{\sqrt{-(16\xi_1\xi_3-5\xi_2^2)}}\right),
\end{aligned} \tag{46}$$

$$S_{11}(x,t) = \pm\sqrt{\frac{-\omega\,(16\xi_1\xi_3-5\xi_2^2)}{\kappa\,\mathfrak{X}}}\, sn\left(\frac{\xi_2}{4\sqrt{\xi_1}}\psi, \frac{\sqrt{-(16\xi_1\xi_3-5\xi_2^2)}}{\xi_2}\right), \tag{47}$$

$$S_{12}(x,t) = \pm\sqrt{\frac{\omega}{\kappa\,\mathfrak{X}}}\,\xi_2\, sn\left(\frac{\sqrt{-\xi_1(16\xi_1\xi_3-5\xi_2^2)}}{4\xi_1}\psi, \frac{\xi_2}{\sqrt{-(16\xi_1\xi_3-5\xi_2^2)}}\right). \tag{48}$$

Case 2: With the parameters $\xi_4 = \frac{\xi_2(4\xi_1\xi_3-\xi_2^2)}{8\xi_1^2}$, $\xi_5 = \frac{(4\xi_1\xi_3-\xi_2^2)^2}{64\xi_1^3}$, the system (34) passes the solution set as follow:

$$\mu_0 = \pm\sqrt{\frac{\omega}{\kappa\,\mathfrak{X}}}\,\xi_2, \quad \mu_1 = \pm 4\sqrt{\frac{\omega}{\kappa\,\mathfrak{X}}}\,\xi_1, \quad \delta = -\frac{k^2\mathfrak{X} + 8\omega\xi_1}{n_0^2\,\mathfrak{X}}, \tag{49}$$

where $\mathfrak{X} = 8\xi_1\xi_3 - 3\xi_2^2$.

Substituting into (33) and using (18)–(21) gives the hyperbolic and trigonometric solutions for (30):

$$S(x,t) = \Psi(\psi) = \pm\sqrt{\frac{\omega}{\kappa\,\mathfrak{X}}}\,\xi_2 + \pm 4\sqrt{\frac{\omega}{\kappa\,\mathfrak{X}}}\,\xi_1 Y(\psi), \tag{50}$$

Sub-case 2.1: If $\xi_1 > 0,\ \mathfrak{X} < 0.$

$$S_{13}(x,t) = \pm\sqrt{\frac{-\omega}{\kappa\,\mathfrak{X}}}\,\xi_2\, \tanh\left(\frac{\sqrt{-\xi_1\mathfrak{X}}}{4\xi_1}\psi\right), \tag{51}$$

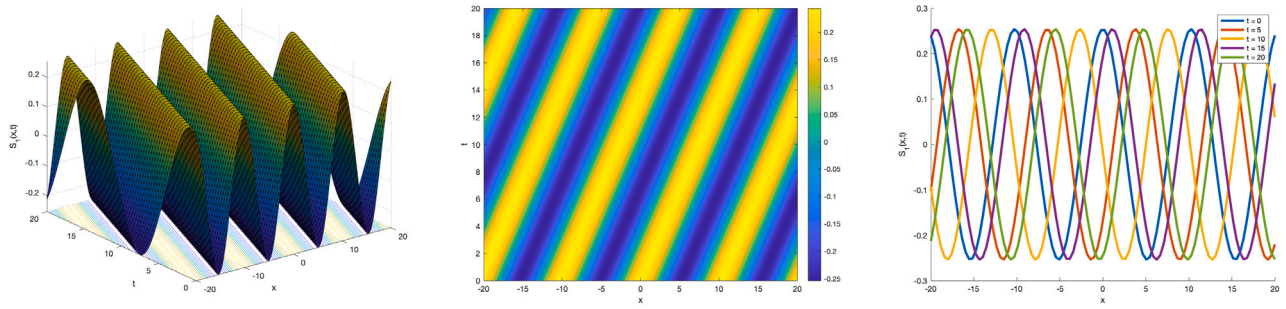

(a) 3-D demonstration (b) 2D-contour (c) 2-D demonstration

Fig. 1. 3D, 2D contour, and 2D representations of elliptic Jacobi solutions of S_1 as periodic waveforms for $\omega = 1.5$, $\kappa = 1.2$, $\xi_1 = 1$, $\xi_2 = 0.5$, $\xi_3 = 0.7$, $n_0 = 0.8$, $k = 0.6$.

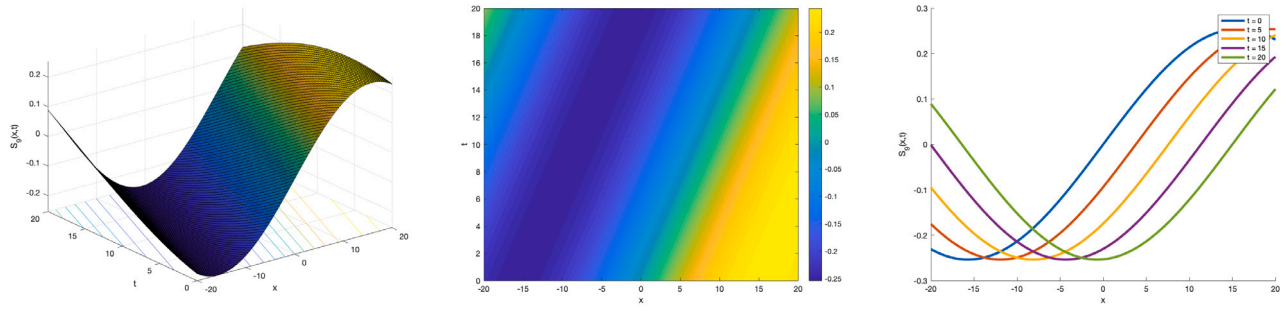

(a) 3-D demonstration (b) 2D-contour (c) 2-D demonstration

Fig. 2. 3D, 2D contour, and 2D representations of elliptic Jacobi solutions of S_9 as dark compacton waveforms for $\omega = 1.5$, $\kappa = 1.2$, $\xi_1 = 1$, $\xi_2 = 0.5$, $\xi_3 = 0.7$, $n_0 = 0.8$, and $k = 0.6$.

$$S_{14}(x,t) = \pm\sqrt{\frac{-\omega}{\kappa\,\mathfrak{X}}}\,\xi_2\,\coth\left(\frac{\sqrt{-\xi_1\mathfrak{X}}}{4\xi_1}\,\psi\right). \tag{52}$$

The kink and singular Kink soliton profiles (51) and (52) are shown in Fig's. 3 and 4.

Sub-case 2.2: If $\xi_1 > 0,\ \mathfrak{X} > 0$.

$$S_{15}(x,t) = \pm\sqrt{\frac{\omega}{\kappa\,\mathfrak{X}}}\,\xi_2\,\tan\left(\frac{\sqrt{\xi_1\mathfrak{X}}}{4\xi_1}\,\psi\right), \tag{53}$$

$$S_{16}(x,t) = \pm\sqrt{\frac{\omega}{\kappa\,\mathfrak{X}}}\,\xi_2\,\cot\left(\frac{\sqrt{\xi_1\mathfrak{X}}}{4\xi_1}\,\psi\right). \tag{54}$$

The periodic solution profiles described in (54) are depicted in Fig. 5.

Case 3: When $\xi_4 = \frac{\xi_2(4\xi_1\xi_3-\xi_2^2)}{8\xi_1^2}$, $\xi_5 = \frac{\xi_2^2(16\xi_1\xi_3-5\xi_2^2)}{256\xi_1^3}$, yields the following the set as a solutions of system (34):

$$\mu_0 = \pm\sqrt{\frac{\omega}{\kappa\,\mathfrak{X}}}\,\xi_2, \quad \mu_1 = \pm 4\sqrt{\frac{\omega}{\kappa\,\mathfrak{X}}}\,\xi_1, \quad \delta = -\frac{k^2\mathfrak{X} + 8\omega\xi_1}{n_0^2\,\mathfrak{X}}, \tag{55}$$

where $\mathfrak{X} = 8\xi_1\xi_3 - 3\xi_2^2$.

Substituting into (33) and applying (22)–(25) gives the hyperbolic and trigonometric solutions for (30):

$$S(x,t) = \Psi(\psi) = \pm\sqrt{\frac{\omega}{\kappa\,\mathfrak{X}}}\,\xi_2 + \pm 4\sqrt{\frac{\omega}{\kappa\,\mathfrak{X}}}\,\xi_1 Y(\psi). \tag{56}$$

Sub-case 3.1: If $\xi_1 < 0,\ \mathfrak{X} < 0$.

$$S_{17}(x,t) = \pm\sqrt{\frac{-2\,\omega}{\kappa\,\mathfrak{X}}}\,\xi_2\,sech\left(\frac{\sqrt{2\xi_1\mathfrak{X}}}{4\xi_1}\,\psi\right). \tag{57}$$

The profiles of the bright soliton solution given by (57) are depicted in Fig. 6.

Sub-case 3.2: If $\xi_1 > 0,\ \mathfrak{X} > 0$.

$$S_{18}(x,t) = \pm\sqrt{\frac{2\,\omega}{\kappa\,\mathfrak{X}}}\,\xi_2\,csch\left(\frac{\sqrt{2\xi_1\mathfrak{X}}}{4\xi_1}\,\psi\right). \tag{58}$$

The profiles of singular soliton solution (58) are illustrated in Fig. 7

Sub-case 3.3: If $\xi_1 > 0,\ \mathfrak{X} < 0$.

$$S_{19}(x,t) = \pm\sqrt{\frac{-2\,\omega}{\kappa\,\mathfrak{X}}}\,\xi_2\,sec\left(\frac{\sqrt{-2\xi_1\mathfrak{X}}}{4\xi_1}\,\psi\right), \tag{59}$$

$$S_{20}(x,t) = \pm\sqrt{\frac{-2\,\omega}{\kappa\,\mathfrak{X}}}\,\xi_2\,csc\left(\frac{\sqrt{-2\xi_1\mathfrak{X}}}{4\xi_1}\,\psi\right). \tag{60}$$

Case 4: Substituting $\xi_2 = \xi_4 = \xi_5 = 0$ and $\xi_3 > 0$ yields a solution to Eq. (34) in the following form:

$$\mu_0 = 0, \quad \mu_1 = \pm\sqrt{\frac{2\,\omega\xi_1}{\kappa\xi_3}}, \quad \delta = -\frac{k^2\xi_3 + \omega}{n_0^2\xi_3}, \tag{61}$$

by substituting these values into Eq. (33) and employing Eq's (26)–(28), the following solution for the generalized reaction Duffing Eq. (30) is derived:

$$S(x,t) = \Psi(\psi) = \pm\sqrt{\frac{2\,\omega\xi_1}{\kappa\xi_3}}\,Y(\psi). \tag{62}$$

$$S_{21}(x,t) = \pm\sqrt{\frac{2\,\omega\xi_1\xi_3}{\kappa}}\,\frac{4\rho}{\left(4\rho^2 e^{\sqrt{\xi_3}\psi} - \xi_1\xi_3 e^{-\sqrt{\xi_3}\psi}\right)}, \tag{63}$$

the profiles of Breather waves solution (63) are illustrated in Fig. 8.

By taking $\xi_1 = -\frac{4\rho^2}{\xi_3}$, solution Eq. (63) reduces to

$$S_{22}(x,t) = \pm\frac{1}{\rho}\sqrt{\frac{\omega\xi_1\xi_3}{2\kappa}}\,sech(-\sqrt{\xi_3}\psi), \tag{64}$$

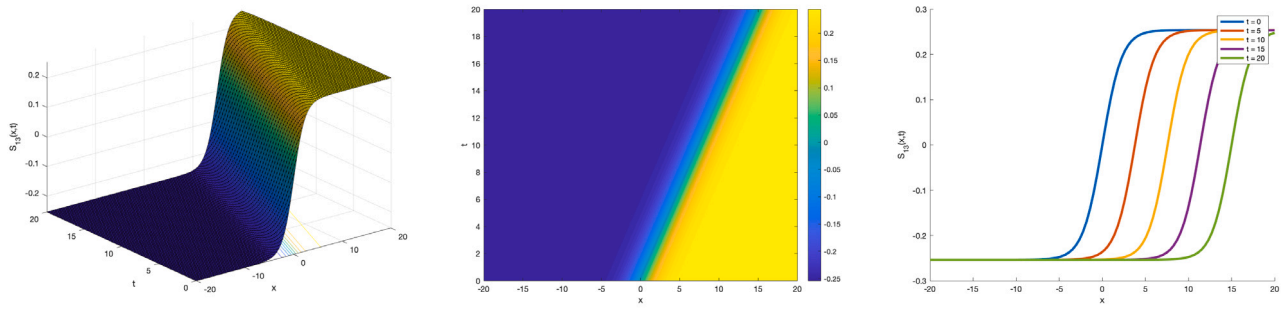

(a) 3-D demonstration (b) 2D-contour (c) 2-D demonstration

Fig. 3. 3D, 2D contour, and 2D representations of S_{13} as kink soliton solutions for $\omega = -1.5$, $\kappa = 1.2$, $\xi_1 = 1$, $\xi_2 = 0.5$, $\xi_3 = 0.7$, $n_0 = 0.8$, and $k = 0.6$.

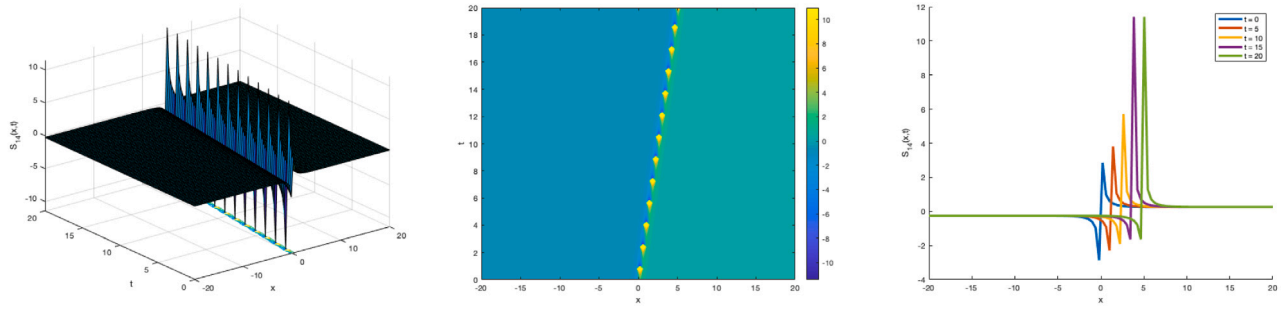

(a) 3-D demonstration (b) 2D-contour (c) 2-D demonstration

Fig. 4. 3D, 2D contour, and 2D representations of S_{14} as a singular kink soliton for $\omega = -1.5$, $\kappa = 1.2$, $\xi_1 = 1$, $\xi_2 = 0.5$, $\xi_3 = 0.7$, $n_0 = 0.8$, and $k = 2.6$.

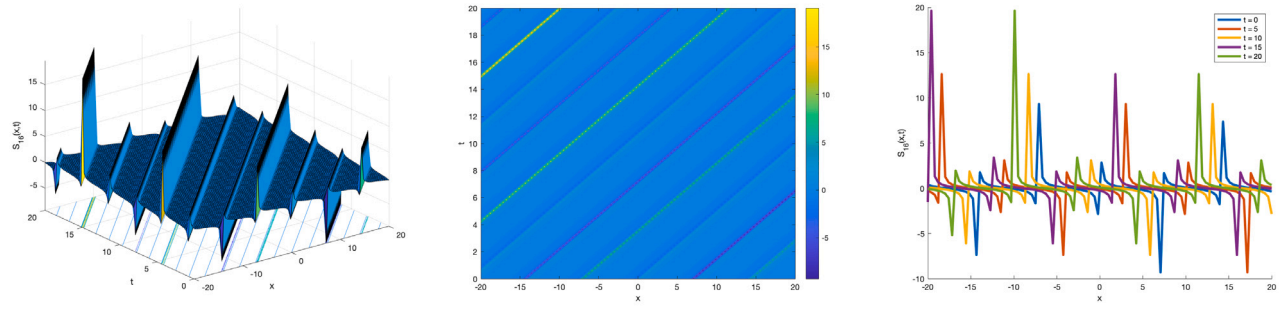

(a) 3-D demonstration (b) 2D-contour (c) 2-D demonstration

Fig. 5. 3D, 2D contour, and 2D representations of S_{16} as periodic solutions for $\omega = 1.5$, $\kappa = 1.2$, $\xi_1 = 1$, $\xi_2 = 0.5$, $\xi_3 = 0.7$, $n_0 = 0.8$, and $k = 1.6$.

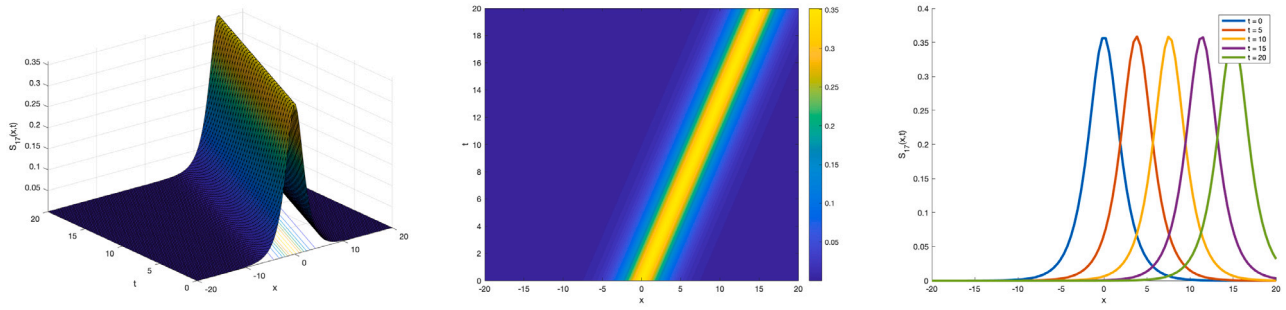

(a) 3-D demonstration (b) 2D-contour (c) 2-D demonstration

Fig. 6. 3D, 2D contour, and 2D representations of S_{17} as a bright soliton for $\omega = -1.5$, $\kappa = 1.2$, $\xi_1 = 1$, $\xi_2 = 0.5$, $\xi_3 = 0.7$, $n_0 = 0.8$, and $k = 0.6$.

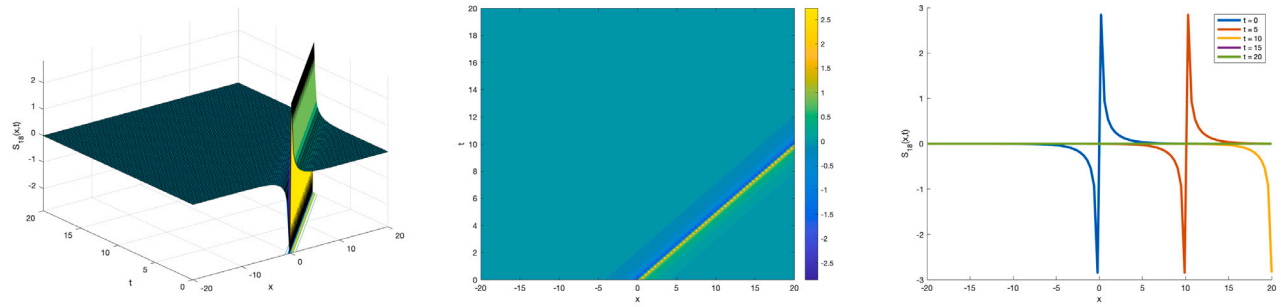

(a) 3-D demonstration (b) 2D-contour (c) 2-D demonstration

Fig. 7. 3D, 2D contour, and 2D representations of S_{18} as a singular soliton form for $\omega = 1.5$, $\kappa = 1.2$, $\xi_1 = 1$, $\xi_2 = 0.5$, $\xi_3 = 0.5$, $n_0 = 0.8$, and $k = 1.6$.

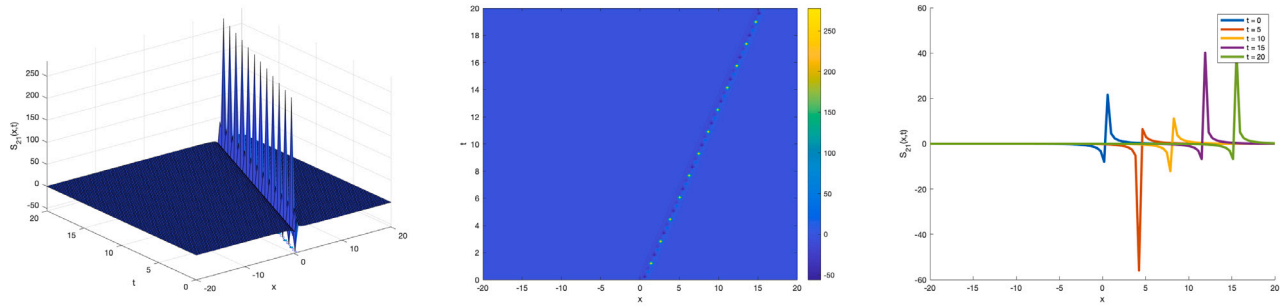

(a) 3-D demonstration (b) 2D-contour (c) 2-D demonstration

Fig. 8. 3D, 2D contour, and 2D representations of S_{21} as breather waveforms for $\omega = 1.5$, $\kappa = 1.2$, $\xi_1 = 1$, $\xi_2 = 0.5$, $\xi_3 = 0.7$, $\rho = 0.3$, $n_0 = 0.8$, and $k = 0.6$.

while by taking $\xi_1 = \frac{4\rho^2}{\xi_3}$, solution Eq. (64) reduces to

$$S_{23}(x,t) = \pm\frac{1}{\rho}\sqrt{\frac{\omega\xi_1\xi_3}{2\kappa}}csch(-\sqrt{\xi_3}\psi). \tag{65}$$

Graphical representation and its behavior

The purpose of this study is to use MATLAB as a computational tool to investigate the graphical characteristics of the generalized reaction Duffing model. The evolution of wave propagation over time at various velocities is depicted using a variety of visual representations, such as 2D contour plots, 3D plots, and 2D graphs. The analysis takes into account a wide range of parameters for the pertinent variables and is conducted within the domains $-20 \le x \le 20$ and $0 \le t \le 20$. The modulus of the Jacobi elliptic function graphs is limited to the interval $[0, 1]$. Exploring the model's graphical behavior in detail and highlighting the dynamics that arise from changing the model's parameters are the main goals. In solving the equation, elliptic Jacobi functions, trigonometric functions, exponential functions, and hyperbolic functions are employed to capture the full range of solutions.

This section presents the behaviors and explanations of several acquired solutions. Fig. 1 presents the elliptic Jacobi solutions as periodic waveforms for the parameters $\omega = 1.5$, $\kappa = 1.2$, $\xi_1 = 1$, $\xi_2 = 0.5$, $\xi_3 = 0.7$, $n_0 = 0.8$, and $k = 0.6$. The solutions exhibit oscillatory behavior, which is characteristic of elliptical functions, since their results are stable and periodic. The features indicate that the system lies between the wave propagation model and the nonlinear wave influence model, suggesting that many factors may interchangeably affect the forms of the waves. Fig. 2 illustrates the elliptic Jacobi solutions of S_9 as dark compacton waveforms, characterized by parameters $\omega = 1.5$, $\kappa = 1.2$, $\xi_1 = 1$, $\xi_2 = 0.5$, $\xi_3 = 0.7$, $n_0 = 0.8$, and $k = 0.6$. The solution behavior demonstrates localized amplitude reductions, showcasing the compact support typical of dark compactons while maintaining stability during propagation. Fig. 3 illustrates the representations of S_{13} as kink soliton solutions for the parameters $\omega = -1.5$, $\kappa = 1.2$, $\xi_1 = 1$, $\xi_2 = 0.5$, $\xi_3 = 0.7$, $n_0 = 0.8$, and $k = 0.6$. The solution behavior demonstrates distinct, sharp transitions indicative of kink formations, highlighting the interplay between the selected parameters and the stability of the soliton profile. These characteristics reveal the essential dynamics of the kink soliton solutions in the specified parameter space. Fig. 4 illustrates the representation of S_{14} as a singular kink soliton for the parameters $\omega = -1.5$, $\kappa = 1.2$, $\xi_1 = 1$, $\xi_2 = 0.5$, $\xi_3 = 0.7$, $n_0 = 0.8$, and $k = 2.6$. A singular Kink soliton, featuring a sharp transition between two states and a localized wave profile associating with the soliton's stability and persistence, exhibits the behavior of a Kink soliton. The nature of such kink solutions is unique in nonlinear dynamics, as seen in this behavior. Fig. 5 presents the representation of S_{16} as periodic solutions for the parameters $\omega = 1.5$, $\kappa = 1.2$, $\xi_1 = 1$, $\xi_2 = 0.5$, $\xi_3 = 0.7$, $n_0 = 0.8$, and $k = 1.6$. As periodic waveforms, they show the stability and recurrence characteristics one would expect for periodic waveforms in nonlinear dynamics and provide a potentially observed periodic soliton behavior. Fig. 6 illustrates the representation of S_{17} as a bright soliton for the parameters $\omega = -1.5$, $\kappa = 1.2$, $\xi_1 = 1$, $\xi_2 = 0.5$, $\xi_3 = 0.7$, $n_0 = 0.8$, and $k = 0.6$. The bright soliton solution has a pronounced peak, showing that it is a localized wave packet that preserves its shape while propagating. The amplitude profile is stable and continuous and reveals a balance between nonlinearity and dispersion. The solution serves as a good representative of a coherent structure that travels without changing its form, which elucidates the basic features of bright solitons in the nonlinear wave dynamics. Fig. 7 presents the representation of S_{18} as a singular soliton solution for the parameters $\omega = 1.5$, $\kappa = 1.2$, $\xi_1 = 1$, $\xi_2 = 0.5$, $\xi_3 = 0.5$, $n_0 = 0.8$, and $k = 1.6$. Moreover, the observed singular soliton behavior exhibits sharp transition in the wave profile, where the steep singularities consist of localized peaks and minimal dispersion. This solution demonstrates the stability typical of singular solitons, maintaining its shape during propagation while exhibiting distinct features such as steep gradients at the edges. The impact of several variables on soliton amplitude and width, which characterize

Table 1

Current solutions	Existing solutions	Reference
$\pm\sqrt{\frac{\Omega}{\kappa\,\mathcal{X}}}\,\xi_2\,cn\left(\frac{\sqrt{-\xi_1(4\xi_1\xi_3-\xi_2^2)}}{2\xi_1}\psi,\frac{\xi_2}{2\sqrt{(4\xi_1\xi_3-\xi_2^2)}}\right)$	$\sqrt{-\frac{q}{s}}\left(\frac{S_1\cos(\sqrt{\Omega\lambda}\eta)+S_2\sin(\sqrt{\Omega\lambda}\eta}{S_1\cos(\sqrt{\Omega\lambda}\eta)-S_2\sin(\sqrt{\Omega\lambda}\eta}\right)$	[40]
$\pm\sqrt{\frac{\Omega}{\kappa\,\mathcal{X}}}\,\xi_2\,dn\left(\frac{\xi_2}{4\sqrt{-\xi_1}}\psi,\frac{2\sqrt{(4\xi_1\xi_3-\xi_2^2)}}{\xi_2}\right)$	$\sqrt{\frac{-2qmn}{s}}\sec\left(\sqrt{-h}(\nu)\right)$	[41]
$\pm\sqrt{\frac{\Omega}{\kappa\,\mathcal{X}}}\,\xi_2\,sn\left(\frac{\sqrt{-\xi_1(16\xi_1\xi_3-5\xi_2^2)}}{4\xi_1}\psi,\frac{\xi_2}{\sqrt{-(16\xi_1\xi_3-5\xi_2^2)}}\right)$	$\sqrt{\frac{-2qmn}{s}}\csc\left(\sqrt{-h}(\nu)\right)$	[41]
$\pm\sqrt{\frac{-\Omega(16\xi_1\xi_3-5\xi_2^2)}{\kappa\,\mathcal{X}}}\,ns\left(\frac{\sqrt{-\xi_1(16\xi_1\xi_3-5\xi_2^2)}}{4\xi_1}\psi,\frac{\xi_2}{\sqrt{-(16\xi_1\xi_3-5\xi_2^2)}}\right)$	$\sqrt{\frac{q}{s\lambda\Omega}}\left(\frac{S_1}{\eta S_1+S_2}\right)$	[40]

The above-mentioned table is presenting the comparison of obtained and existing solutions.

the intricate dynamics of wave interactions in this context, is shown. Fig. 8 illustrates the representation of S_{21} as breather waveforms for the parameters $\omega = 1.5$, $\kappa = 1.2$, $\xi_1 = 1$, $\xi_2 = 0.5$, $\xi_3 = 0.7$, $\rho = 0.3$, $n_0 = 0.8$, and $k = 0.6$. Breather soliton solutions display oscillatory behavior and have localized temporal peaks that fluctuate, illustrating the dynamic interaction between wave amplitude and forward wave propagation. The stability and durability of these breather solitons highlight their significance in nonlinear wave processes.

The diversity of soliton solutions is helpful for future research, as it reduces the complexity of systems used in several scientific domains, such as fluid dynamics, optical fibers, and condensed matter physics, hence facilitating advancements in practical and theoretical development.

Comparison

This section will present the comparison of obtained results with existing solutions (see Table 1). The above-mentioned table is presenting the comparison of obtained and existing solutions.

Chaotic analysis

In this section, the chaos analysis will be discussed because the chaotic analysis of differential systems provides valuable insights into the behavior of complex systems, enhancing our ability to predict, control, and optimize processes across various scientific and engineering domains. Recently, Wang et al. [47] presented the chaotic analysis for modified Camassa–Holm equation and displayed quasi-periodic and chaotic behaviors of the system and explained their applicability. For discussing the chaotic analysis of the studied equation, consider $\Psi' = G$ and Eq. (32), with perturbation term can be expressed as follows:

$$\begin{aligned}\frac{d\Psi}{d\psi} &= G,\\ \frac{dG}{d\psi} &= -\frac{\Psi(\omega+\kappa\Psi^2)}{\kappa^2+\delta n_0^2}+\Omega(\psi),\end{aligned} \tag{66}$$

where $\Omega = \alpha\cos\beta t$ is a perturbation term, and represents the outward periodic force, α and β depict the frequency and intensity of periodic phrase respectively. In our research, we observed chaotic behavior in system (66), characterized by unpredictable time-dependent trajectories diverging from regular patterns. To detect chaos, we employed 2D phase portrait, Poincare map, and time series analysis by giving the values of the suitable parameters. The graphs for the dynamical system (66), are shown in Figs. 9 and 10.

Conclusion

In this study, we construct novel traveling wave solutions for the generalized reaction Duffing model using the Kumar–Malik approach. This strategy consistently yields more thorough, creative, and precise solutions than other approaches, exhibiting notable advantages. In conclusion, a variety of soliton solutions have been established, such as breather waves, bright solitons, periodic wave solutions, dark compacton wave solutions, kink waves, singular kink waves, and singular shape soliton solutions. Graphical representations of these traveling wave solutions are provided, with their accuracy confirmed using a basic computational program in MATLAB 2022. Both 2D and 3D visualizations effectively illustrate the dynamic behavior of the observed solutions. The established wave solutions exhibit greater generality than those previously reported in the literature, with distinct parameter values identified and several known solutions recovered. Furthermore, the effect of varying the k parameter, which indicates soliton velocity, is clearly illustrated. This study highlights the efficiency, clarity, coherence, and consistency of the Kumar–Malik method, revealing several novel traveling wave solutions that have not been observed before. The proposed methodology also allows for the assessment of stability and applicability in other nonlinear evolution equations, suggesting further research opportunities. The dynamics of the model under slight variation have been rigorously investigated by the inclusion of perturbation terms and a rigorous definition of initial conditions in the chaotic analysis. Future applications of this approach may extend to exploring traveling wave solutions in quantum mechanics, engineering, neurology, and ophthalmology. The effectiveness of the Kumar–Malik method in obtaining exact solutions has been validated across various studies. The researchers could look into and use this study further to visualize additional dynamical characteristics of the physical processes. The power spectrum and return map tools can be used in future studies to examine the model in further detail. Breathers, rogue waves, numerous solitons, and their interaction can all be described by different processes, including the Hirota bilinear technique.

CRediT authorship contribution statement

Ghulam Hussain Tipu: Writing – original draft, Software, Resources, Methodology, Investigation, Formal analysis. **Waqas Ali Faridi:** Supervision, Investigation, Data curation. **Muhammad Bilal Riaz:** Funding acquisition, Formal analysis. **Fengping Yao:** Supervision, Methodology. **Usman Younas:** Supervision, Methodology, Data curation. **Mubariz Garayev:** Software, Project administration.

Consent for publication

Not applicable

Ethics approval and consent to participate

Not applicable

Declaration of competing interest

All the authors hereby declare that they have no conflict of interest in submission the paper titled.

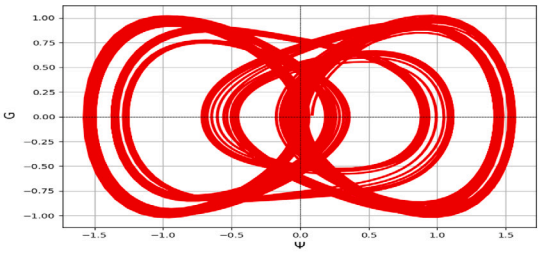

(a) $\alpha = 0.7, \beta = 0.1$

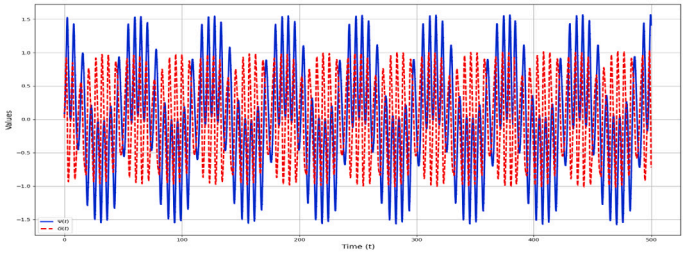

(b) $\alpha = 0.7, \beta = 0.1$

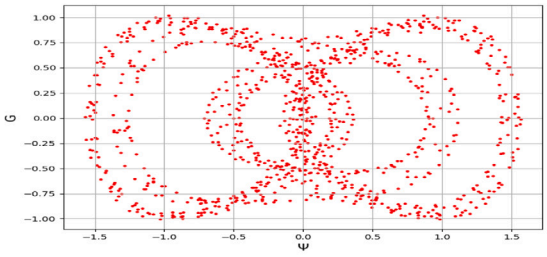

(c) $\alpha = 0.7, \beta = 0.1$

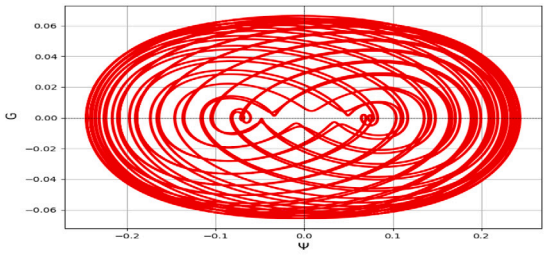

(d) $\alpha = 0.008, \beta = 0.23$

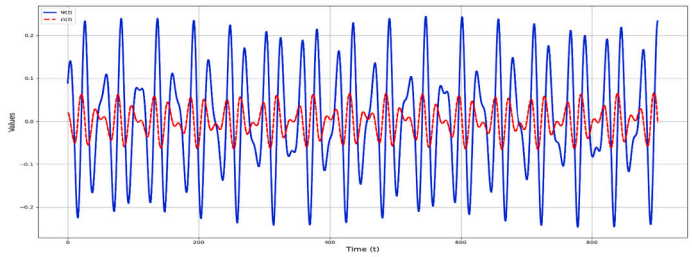

(e) $\alpha = 0.008, \beta = 0.23$

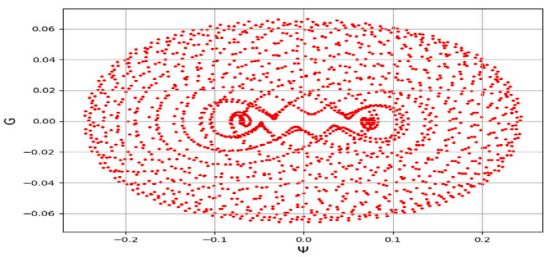

(f) $\alpha = 0.008, \beta = 0.23$

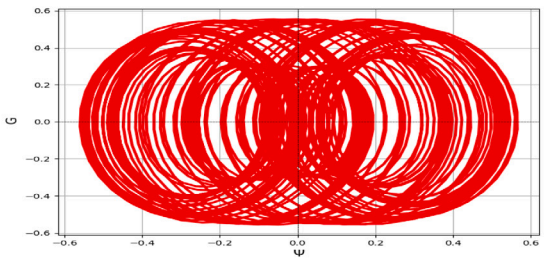

(g) $\alpha = 0.8, \beta = 1.93$

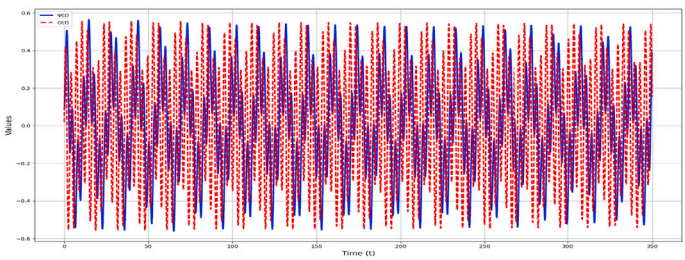

(h) $\alpha = 0.8, \beta = 1.93$

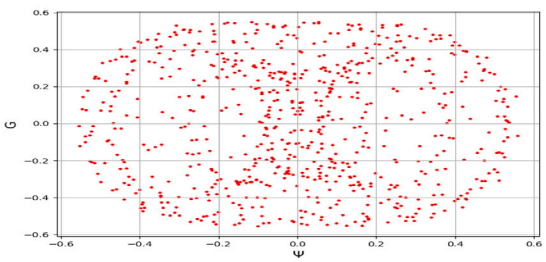

(i) $\alpha = 0.8, \beta = 1.93$

Fig. 9. Plots for chaos in system (66) using 2D phase portrait, time analysis and Poincare maps with $\kappa = 1.5, \delta = .01, n_0 = .9, \omega = .2$, and taking the initial conditions $(0.02, 0.089)$.

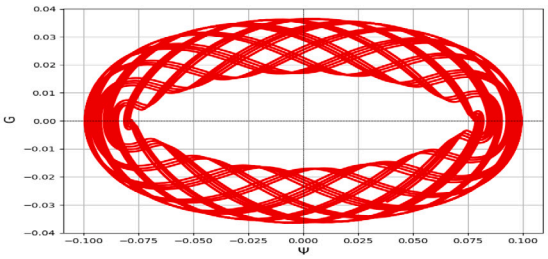

(a) $\alpha = 0.009, \beta = 0.1$

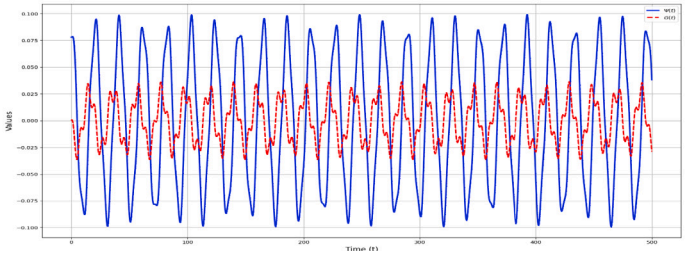

(b) $\alpha = 0.009, \beta = 0.1$

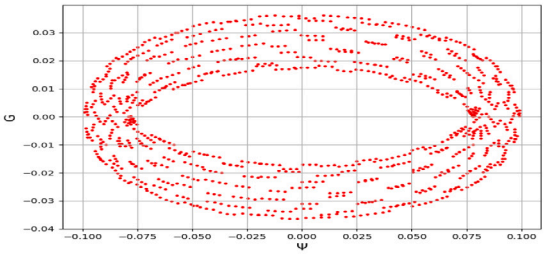

(c) $\alpha = 0.009, \beta = 0.1$

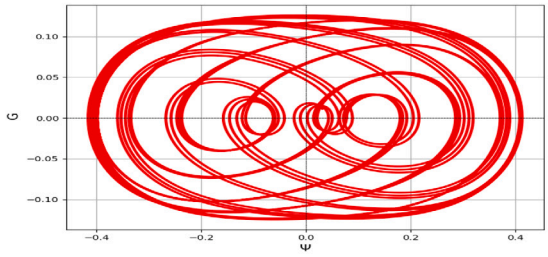

(d) $\alpha = 0.02, \beta = 0.23$

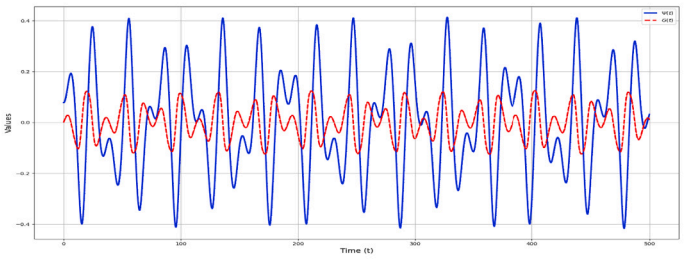

(e) $\alpha = 0.02, \beta = 0.23$

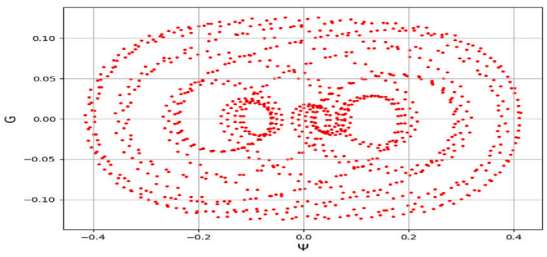

(f) $\alpha = 0.02, \beta = 0.23$

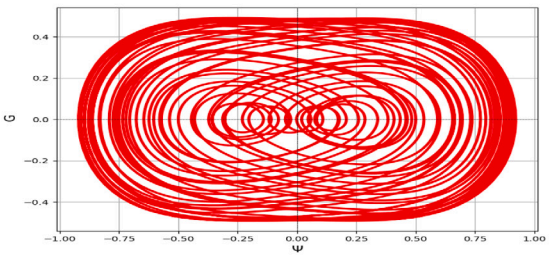

(g) $\alpha = 0.06, \beta = 0.44$

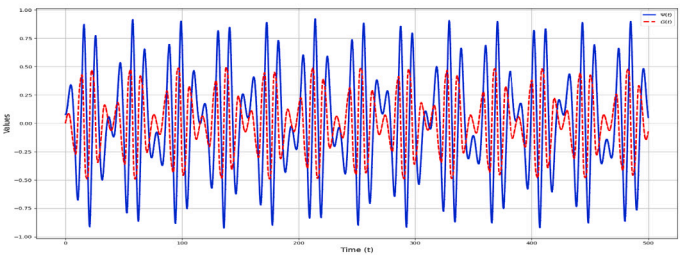

(h) $\alpha = 0.06, \beta = 0.44$

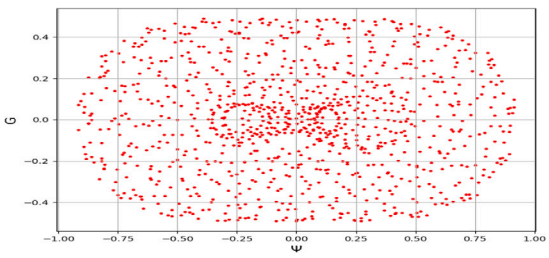

(i) $\alpha = 0.06, \beta = 0.44$

Fig. 10. Plots for chaos in system (66) using 2D phase portrait, time analysis and Poincare maps with $\kappa = 1.5, \delta = .01, n_0 = .9, \omega = .2$, and taking the initial conditions $(0, 0.078)$.

Acknowledgments

The authors extend their appreciation to King Saud University, Saudi Arabia for funding this work through Researchers Supporting Project number ($RSPD2025R1056$), King Saud University, Riyadh, Saudi Arabia. No funding available. This article has been produced with the financial support of the European Union under the REFRESH – Research Excellence For Region Sustainability and High-tech Industries project number CZ.10.03.01/00/22_003/0000048 via the Operational Programmed Just Transition.

Data availability

No data was used for the research described in the article.

References

[1] Isah Muhammad Abubakar, Külahcı Mihriban Alyamaç. A study on null cartan curve in Minkowski 3-space. Appl Math Nonlinear Sci 2020;5(1):413–24.
[2] Isah Muhammad Abubakar, Külahçı Mihriban Alyamaç. Special curves according to bishop frame in minkowski 3-space. Appl Math Nonlinear Sci 2020;5(1):237–48.
[3] Kumar Amit, Kumar Sachin, Kharbanda Harsha. Closed-form invariant solutions from the Lie symmetry analysis and dynamics of solitonic profiles for (2+ 1)-dimensional modified heisenberg ferromagnetic system. Modern Phys Lett B 2022;36(07):2150609.
[4] Kumar Sachin, Hamid Ihsanullah, Abdou MA. Specific wave profiles and closed-form soliton solutions for generalized nonlinear wave equation in (3+ 1)-dimensions with gas bubbles in hydrodynamics and fluids. J Ocean Eng Sci 2023;8(1):91–102.
[5] Yokus Asıf, Isah Muhammad Abubakar. Stability analysis and soliton solutions of the nonlinear evolution equation by homoclinic technique based on Hirota bilinear form. In: 2023 international conference on fractional differentiation and its applications. ICFDA, IEEE; 2023, p. 1–6.
[6] Spiegelman Marc. Geochemical effects of magmatic solitary waves—II. Some analysis. Geophys J Int 1994;117(2):296–300.
[7] Davies Adeyemo Oke, Khalique Chaudry Masood. Computational approach in obtaining analytic solutions of a generalized nonlinear breaking soliton equation with applications in engineering and physics. J Taibah Univ Sci 2024;18(1):2331984.
[8] Faridi Waqas Ali, Iqbal Mujahid, Riaz Muhammad Bilal, AlQahtani Salman A, Wazwaz Abdul-Majid. The fractional soliton solutions of dynamical system arising in plasma physics: The comparative analysis. Alex Eng J 2024;95:247–61.
[9] Mohan Brij, Kumar Sachin. Generalization and analytic exploration of soliton solutions for nonlinear evolution equations via a novel symbolic approach in fluids and nonlinear sciences. Chinese J Phys 2024;92:10–21.
[10] Ahmad Imran, Faridi Waqas Ali, Iqbal Mujahid, Majeed Zain, Tchier Fairouz. Exploration of soliton solutions in nonlinear optics for the third order Klein–Fock–Gordon equation and nonlinear Maccari's system. Internat J Theoret Phys 2024;63(6):157.
[11] Liu Xiaoyan, Zhang Hongxin, Liu Wenjun. The dynamic characteristics of pure-quartic solitons and soliton molecules. Appl Math Model 2022;102:305–12.
[12] Kumar Chandan, Prakash Akshay. Nonlinear interaction among second mode resonance waves in high-speed boundary layers using the method of multiple scales. Phys Fluids 2022;34(1).
[13] Zhang Chuanhong, Shi Zhiwei. Nonlinear wave interactions in a transitional hypersonic boundary layer. Phys Fluids 2022;34(11).
[14] Tipu Ghulam Hussain, Faridi Waqas Ali, Rizk Doaa, Myrzakulova Zhaidary, Myrzakulov Ratbay, Akinyemi Lanre. The optical exact soliton solutions of Shynaray-IIA equation with Φ^6−model expansion approach. Opt Quantum Electron 2024;56(2):226.
[15] Asjad Muhammad Imran, Faridi Waqas Ali, Alhazmi Sharifah E, Hussanan Abid. The modulation instability analysis and generalized fractional propagating patterns of the Peyrard–Bishop DNA dynamical equation. Opt Quantum Electron 2023;55(3):232.
[16] Faridi Waqas Ali, Asjad Muhammad Imran, Jarad Fahd. Non-linear soliton solutions of perturbed Chen–Lee–Liu model by ϕ^6−model expansion approach. Opt Quantum Electron 2022;54(10):664.
[17] Zayed Elsayed ME, Al-Nowehy Abdul-Ghani, Elshater Mona EM. New-model expansion method and its applications to the resonant non-linear Schrödinger equation with parabolic law non-linearity. Eur Phys J Plus 2018;133(10):417.
[18] Rizvi Syed TR, Seadawy Aly R, Ali K, Younis M, Ashraf MA. Multiple lump and rogue wave for time fractional resonant non-linear Schrödinger equation under parabolic law with weak nonlocal non-linearity. Opt Quantum Electron 2022;54(4):212.
[19] Kumar Sachin, Mohan Brij, Kumar Raj. Lump, soliton, and interaction solutions to a generalized two-mode higher-order non-linear evolution equation in plasma physics. Non-Linear Dyn 2022;110(1):693–704.
[20] Das Nilkanta, Saha Ray S. Investigations of bright, dark, kink-antikink optical and other soliton solutions and modulation instability analysis for the (1+ 1)-dimensional resonant nonlinear Schrödinger equation with dual-power law nonlinearity. Opt Quantum Electron 2023;55(12):1071.
[21] Malik Sandeep, Hashemi Mir Sajjad, Kumar Sachin, Rezazadeh Hadi, Mahmoud W, Osman MS. Application of new kudryashov method to various non-linear partial differential equations. Opt Quantum Electron 2023;55(1):8.
[22] Ur Rahman Riaz, Faridi Waqas Ali, El-Rahman Magda Abd, Taishiyeva Aigul, Myrzakulov Ratbay, Az-Zo'bi Emad Ahmad. The sensitive visualization and generalized fractional solitons' construction for regularized long-wave governing model. Fractal Fract 2023;7(2):136.
[23] Wazwaz Abdul-Majid, El-Tantawy SA. Bright and dark optical solitons for (3+ 1)-dimensional hyperbolic non-linear Schrödinger equation using a variety of distinct schemes. Optik 2022;270:170043.
[24] Arnous Ahmed H, Mirzazadeh Mohammad, Akinyemi Lanre, Akbulut Arzu. New solitary waves and exact solutions for the fifth-order nonlinear wave equation using two integration techniques. J Ocean Eng Sci 2023;8(5):475–80.
[25] Zafar Asim, Shakeel Muhammad, Ali Asif, Akinyemi Lanre, Rezazadeh Hadi. Optical solitons of non-linear complex Ginzburg–Landau equation via two modified expansion schemes. Opt Quantum Electron 2022;54:1–15.
[26] Das Nilkanta, Saha Ray S. Exact traveling wave solutions and soliton solutions of conformable M-fractional modified nonlinear Schrödinger model. Optik 2023;287:171060.
[27] Elsherbeny Ahmed M, Mirzazadeh Mohammad, Akbulut Arzu, Arnous Ahmed H. Optical solitons of the perturbation Fokas–Lenells equation by two different integration procedures. Optik 2023;273:170382.
[28] Nisar Kottakkaran Sooppy, Akinyemi Lanre, Inc Mustafa, Şenol Mehmet, Mirzazadeh Mohammad, Houwe Alphonse, Abbagari Souleymanou, Rezazadeh Hadi. New perturbed conformable Boussinesq-like equation: Soliton and other solutions. Results Phys 2022;33:105200.
[29] Akinyemi Lanre, Şenol Mehmet, Osman MS. Analytical and approximate solutions of non-linear Schrödinger equation with higher dimension in the anomalous dispersion regime. J Ocean Eng Sci 2022;7(2):143–54.
[30] Khater Mostafa MA. Multi-vector with nonlocal and non-singular kernel ultrashort optical solitons pulses waves in birefringent fibers. Chaos Solitons Fractals 2023;167:113098.
[31] Khater Mostafa MA. Non-linear biological population model; computational and numerical investigations. Chaos Solitons Fractals 2022;162:112388.
[32] Singh Shailendra, Saha Ray S. New analytical solutions and integrability for the (2+ 1)-dimensional variable coefficients generalized Nizhnik–Novikov–Veselov system arising in the study of fluid dynamics via auto-backlund transformation approach. Phys Scr 2023;98(8):085243.
[33] Tarla Sibel, Ali Karmina K, Yilmazer Resat, Osman MS. New optical solitons based on the perturbed Chen–Lee–Liu model through Jacobi elliptic function method. Opt Quantum Electron 2022;54(2):131.
[34] Tarla Sibel, Ali Karmina K, Sun Tian-Chuan, Yilmazer Resat, Osman MS. Nonlinear pulse propagation for novel optical solitons modeled by fokas system in monomode optical fibers. Results Phys 2022;36:105381.
[35] Shaikh Tahira Sumbal, Baber Muhammad Zafarullah, Ahmed Nauman, Iqbal Muhammad Sajid, Akgül Ali, El Din Sayed M. Acoustic wave structures for the confirmable time-fractional Westervelt equation in ultrasound imaging. Results Phys 2023;49:106494.
[36] Kovacic Ivana, Brennan Michael J. The duffing equation: nonlinear oscillators and their behaviour. John Wiley & Sons; 2011.
[37] Long-Jye Sheu, Hsien-Keng Chen, Juhn-Horng Chen, Lap-Mou Tam. Chaotic dynamics of the fractionally damped duffing equation. Chaos Solitons Fractals 2007;32:1459–68.
[38] Vivas-Cortez Miguel, Aftab Maryam, Abbas Muhammad, Alosaimi Moataz. Abundant soliton solutions to the generalized reaction duffing model and their applications. Symmetry 2024;16(7):847.
[39] Tariq Kalim U, Inc Mustafa, Hashemi Mir Sajjad. On the soliton structures to the space–time fractional generalized reaction duffing model and its applications. Opt Quantum Electron 2024;56(4):708.
[40] Razzaq W, Zafar A, Bekir A. Traveling wave solutions of some CFD reaction duffing and diffusion–reaction equations arising in mathematical physics. Int J Appl Comput Math 2024;10(3):107.
[41] Said Ameer, Bakkar Abu, Khan Hassan, Cattani Carlo, Tchier Fairouz. Construction of mechanically preserved optical travelling wave solution for fractional generalized reaction duffing model. J Appl Comput Mech 2025.
[42] Kumar Sachin, Malik Sandeep. A new analytic approach and its application to new generalized Korteweg–de Vries and modified Korteweg–de Vries equations. Math Methods Appl Sci 2024.
[43] Wang Kang-Jia. The generalized (3+ 1)-dimensional B-type Kadomtsev–Petviashvili equation: resonant multiple soliton, N-soliton, soliton molecules and the interaction solutions. Nonlinear Dynam 2024;112(9):7309–24.

[44] Wang Kang-Jia. N-soliton, soliton molecules, Y-type soliton, periodic lump and other wave solutions of the new reduced B-type Kadomtsev–Petviashvili equation for shallow water waves. Eur Phys J Plus 2024;139(3):1–13.
[45] Chou Dean, Boulaaras Salah Mahmoud, Rehman Hamood Ur, Iqbal Ifrah, Akram Asma, Ullah Naeem. Additional investigation of the Biswas–Arshed equation to reveal optical soliton dynamics in birefringent fiber. Opt Quantum Electron 2024;56(4):705.
[46] Chou Dean, Rehman Hamood Ur, Amer Aamna, Amer Aatika. New solitary wave solutions of generalized fractional Tzitzéica-type evolution equations using sardar sub-equation method. Opt Quantum Electron 2023;55(13):1148.
[47] Wang Kang-Jia, Wang Guo-Dong, Shi Feng, Liu Xiao-Lian, Zhu Hong-Wei. Variational principle, Hamiltonian, bifurcation analysis, chaotic behaviors and the diverse solitary wave solutions of the simplified modified Camassa–Holm equation. Int J Geom Methods Mod Phys 2025;2550013.